Analyst

ROYAL SOCIETY OF CHEMISTRY

PAPER

View Article Online
View Journal | View Issue

Cite this: *Analyst*, 2021, **146**, 1668

Entropy-driven amplification strategy-assisted lateral flow assay biosensor for ultrasensitive and convenient detection of nucleic acids†

Shasha Li,[a] Hong-Min Meng, *[a] Hong Zong,[b] Juan Chen,[a] Jianjun Li,*[a] Lin Zhang[a] and Zhaohui Li *[a]

Received 24th November 2020,
Accepted 17th December 2020

DOI: 10.1039/d0an02273j

rsc.li/analyst

Accurate, sensitive and rapid nucleic acid tests are important to implement timely treatment measures and control the spread of disease. Herein, we developed a novel portable platform for highly sensitive and specific detection of nucleic acids by integrating an entropy-driven amplification strategy into lateral flow assay (LFA) biosensor. We find that introducing an entropy-driven amplification strategy yields bright intensities on the test line of LFA stirp, which results in improved sensitivity for targeted nucleic acid detection. The developed LFA biosensor showed good reproducibility, specificity and sensitivity for target DNA and H1N1-RNA detection with a low detection limit of 1.43 pM and 2.02 pM, respectively. Its practical potential was also verified by detecting the target nucleic acid in human serum. More importantly, the design of an entropy-driven amplification strategy in this portable platform retained the convenient, rapid and low-cost characterizations of LFA biosensor due to the compact amplification principle and the elimination of enzyme use. Thus, we believe that this assay biosensor will certainly report its own position in the timely detection of nucleic acid, especially when the medical environment and resources are fewer.

Introduction

Nucleic acid detection is a vital research topic for biochemical analysis and disease diagnostics.[1] In the case of viruses, the RNAs appear much earlier than the antibodies,[2] thus they are considered as exquisite biomarkers for the early diagnosis of various viral diseases, such as influenza,[3,4] severe acute respiratory syndrome (SARS)[5,6] and coronavirus disease 2019 (COVID-19).[7,8] Not only that, many other fields, which include gene profiling,[9,10] forensic analysis[11] and environmental analysis,[12,13] as well as cover the detection of nucleic acids. Although impressive progresses have been made in nucleic acid assay, most of the developed detection manners suffer from high requirement of large-scale equipment, high cost or laborious operation procedure.[14,15] Hence, it is urgently important to develop convenient, rapid and low-cost diagnostic tools for nucleic acids without the sacrifice of sensitivity and accuracy.[16,17]

To satisfy the demands of convenience, rapidness and low-cost, studies on nucleic acids assay have flourished to develop the diversified point of care (POC) diagnostic devices.[18,19] Amongst the different types of POC devices, the lateral flow assay (LFA) biosensor is very prominent, which greatly simplifies the detection procedure and minimizes the cost for making it accessible to resource-poor countries.[12,20] At the early stage, the LFA biosensors established on the basis of various simple visualization methods have been implemented to realize the accurate nucleic acid assay.[21–23] However, the sensitivities of these traditional LFAs need to be improved. On this context, several signal amplification strategies including polymerase chain reaction (PCR),[16,24] rolling circle amplification (RCA)[25] have been combined with LFA biosensors for low-abundant nucleic acid biomarker detection. These studies have one thing in common, they all use various enzymes to realize the signal amplification, which thus increases cost. Furthermore, the introduction of signal amplification strategies such as real-time PCR in some studies leads to the complication of operational procedures.[26] Obviously, these above-mentioned changes seem to deviate from the initial spirit of LFA biosensors, which hinder the wide application of LFA biosensors in household and clinical diagnosis.

As a novel isothermal nucleic acid amplification method, entropy-driven amplification strategy has been recently developed for highly selective and sensitive nucleic acid detection.[27–29] For instance, our group has fabricated an entropy-driven DNA

[a]*College of Chemistry, Green Catalysis Center, Henan Joint International Research Laboratory of Green Construction of Functional Molecules and Their Bioanalytical Applications, Zhengzhou Key Laboratory of Functional Nanomaterial and Medical Theranostic, Zhengzhou University, Zhengzhou 450001, China*
[b]*Department of oncology, The First Affiliated Hospital of Zhengzhou University, Zhengzhou 450052, China*

†Electronic supplementary information (ESI) available. See DOI: 10.1039/d0an02273j

amplification-based nanoprobe for multiplexed detection and imaging of intracellular mRNA.[30] In a typical entropy-driven amplification system, no enzyme is involved, and only several linear single strand DNAs are introduced to play various roles in a catalytic circuit *via* a toehold-assisted branch migration.[31] Unlike the catalytic hairpin assembly[32] and hybridization chain reaction,[33] this hairpin-free amplification strategy is driven by entropy increases in the system rather than the formation of new base pairs, which render it become simpler and more convenient.[34,35] Moreover, the total number of base pairs of the entropy-driven system remains unchanged during the whole amplification process, which reduces the chance of circuit leakage for improving sensitivity and reliability. Thus, employing entropy-driven amplification strategy in LFA biosensors should be a promising option because such arrangement would improve the detection sensitivity while it preserves the convenient, rapid and low-cost characterizations of the LFA biosensor.

Herein, we integrated an entropy-driven amplification technology with an LFA biosensor for the ultrasensitive detection of nucleic acids. As illustrated in Scheme 1, the biotin-labelled S is a three stranded substrate complex (R/L/P) and the strand R is a reporter DNA labelled by a fluorescent nanosphere (FN) at the 5′-end. In the presence of the target, the cascade strand displacement reaction is triggered *via* toehold displacement, which leads to the production of strand R, and is then captured on the test line *via* the hybridization with the capture strand on the test line. Furthermore, the excess biotin-labelled S is captured on the control line *via* a combination with streptavidin (SA). In this strategy, one target can trigger the release of strand R in large quantities by recycling the target, and then the amplified fluorescence of nanosphere produced on the test line can be easily read out by a handheld fluorescence biosensor reader. Compared with the non-amplified assay biosensor, the limit of detection of this LFA biosensor is improved 746 times. Moreover, this LFA biosensor is effective to detect target DNA and H1N1-RNA in real human serum samples, which highlights its application potential in clinical diagnosis.

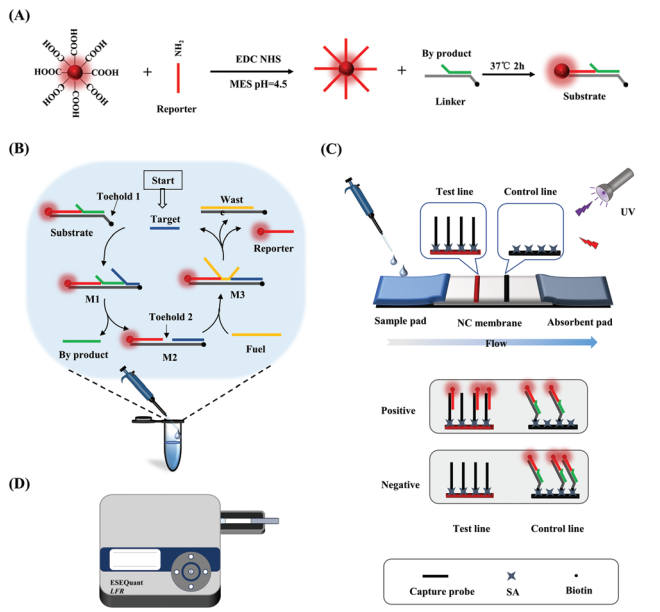

Scheme 1 Schematic presentation (A) the process of preparation of FNs–S conjugates, (B) the FNs-labelled entropy-driven amplification process, (C) the lateral flow assay biosensor for detection of target DNA, (D) the portable device for quantification of lateral flow assay biosensor.

Experimental

Reagents and materials

Carboxyl-functionalized fluorescent nanospheres were provided by Madenw Biotech Co., Ltd (Changsha, China). Nitrocellulose membranes, sample pads, absorption pads and plastic adhesive backing pads were purchased from Goldbio Tech. Co., Ltd (Shanghai, China). 1-Ethyl-3-(3-dimethylaminopropyl)-carbodiimide hydrochloride (EDC), N-hydroxy succinimide (NHS), sodium dodecyl sulfate (SDS) and Tween 20 were obtained from J&K Scientific Co., Ltd (Beijing, China). 2-(N-morpholine) ethane sulfonic acid (MES) powders were obtained from Aladdin reagent Co., Ltd (Shanghai, China). SYBR Gold was gained from Thermo Fisher Scientific (USA). Ultrapure water was prepared from a Millipore Milli-Q water purification system (MA, USA) with an electric resistance of ≥18.2 MΩ cm. Phosphate-buffered saline (PBS) and oligonucleotides were synthesized by Sangon Biotech Co., Ltd (Shanghai, China). The sequences of these oligonucleotides are listed in Table S1.†

Instruments

The size distribution and zeta potential of FNs and FNs-DNA were measured on a Malvern Zetasizer Nano ZS90 (UK). Native gel electrophoresis was imaged on a ChemiDoc XRS system (Bio-Rad, USA). Biosensor cutter-CTS300 and XYZ three-dimensional films spraying gold instrument-HM3035 were obtained from Goldbio Tech Co., Ltd (Shanghai, China) and were used to prepare LFA biosensors. The portable ESEQuant lateral flow reader used to record the fluorescence intensity of the biosensor was provided by Qiagen (Stockach, Germany). The images of FNs and the test biosensors under an UV lamp were taken by a Canon digital camera (Japan).

Preparation of FNsDNA conjugates

The FNs–DNA conjugates were prepared using a previously published procedure with minor modifications.[36] As shown in Scheme 1A, 10 μL of the carboxyl-functionalized FNs stored solution was first centrifuged at 10 012*g* for 40 min at 4 °C. After removing the supernatant, 100 μL of MES buffer (0.1 M, pH 4.5), 2.5 μL of amine-modified DNA and 10 μL of freshly prepared EDC (10 mg mL^{-1}) were added. Furthermore, 30 min later, another 5 μL of EDC was added to the mixture and incubated for another 30 min. Then, 1 mL of 0.02% Tween-20 was added and followed by centrifugation at 13 628*g* for 40 min at

4 °C. The supernatant was removed and the deposit was resuspended in 1 mL of 0.03% sodium dodecyl sulfate (SDS), followed by centrifugation at 13 628*g* for 40 min at 4 °C. Finally, the supernatant was removed and the deposit was resuspended with 100 μL of PBS (pH 7.2), and the obtained solution was maintained at 4 °C for further use.

Fabrication of lateral flow assay biosensor

The typical lateral flow assay biosensor consists of sample pad, conjugate pad, nitrocellulose (NC) membrane, and absorbent pad. Herein, the test line and control line on the NC membrane were prepared by dispensing streptavidin-biotinylated capture DNA and streptavidin, respectively. Moreover, 80 μM capture DNA was first mixed with 1.0 mg mL^{-1} streptavidin and incubated at room temperature for 1 h and then dropped on the test line. The NC membrane was dried in a vacuum oven at 37 °C for 2 h. Then, the sample pad, conjugate pad, NC membrane, and absorbent pad were assembled onto plastic adhesive backing in an orderly manner with an overlap of 2 mm to ensure migration of the sample solution during the testing process. Finally, the obtained plate was cut into 4 mm wide and stored at 4 °C in a dry and dark environment for additional assay.

Preparation of entropy-driven reaction sample

The linker strand (L) and by product strand (P) were pretreated by annealing at 95 °C for 5 min and 4 °C for 10 min, and then they were mixed with reporter strand (R) at 37 °C for 2 h to obtain the substrate complex (S). Then, S, fuel strand (F) and different concentrations of target DNA (T) were mixed together at room temperature for 3 h. The obtained entropy-driven sample was directly loaded on the sample pad for target detection.

Polyacrylamide gel electrophoresis

Seven samples are prepared for gel electrophoresis, and the detailed information for these samples are listed below: (1) 10 μL Marker, (2) 1 μM S, (3) 1 μM S and 1 μM T, (4) 1 μM M2 (R + T + L), (5) 1 μM S, 1 μM F and 0.1 μM T, (6) 1 μM S and 1 μM F, (7) 1 μM W (F + L). After incubation at room temperature for 3 h, these samples with 1× loading buffer and SYBR Gold were applied to 12% polyacrylamide gel electrophoresis with 1× TBE buffer (4.5 mM Tris, 4.5 mM boric acid and 0.1 mM EDTA, pH 7.9) at 4 °C. Electrophoresis was performed at 200 V for 10 min and then 80 V for 1 h in the dark. Then, the images were acquired using a gel imaging system.

Detection of target DNA

The entropy-driven sample solution with different concentrations of target DNA was diluted with PBST buffer (PBS containing 1% tween-20) and then loaded on the sample pad. After 30 min, these biosensors were inserted into the fluorescence biosensor reader to record the value of peak area (Scheme 1D). Then, these biosensors were placed under UV light, and the corresponding fluorescence images were captured by a digital camera. For selectivity assay, single-base substitution sequences mT, mG, mC, insertion sequences iA, iT, iG, iC and deletion sequence dA were incubated with the entropy-driven sample solution. For investigating the application in real sample, the blood was first centrifuged at 15 644*g* for 3 min and then diluted 100 times with PBS. Different concentrations of target DNA were spiked in diluted serum samples and were tested according to that in buffer.

Results and discussion

Principle of the lateral flow assay biosensor

Herein, we combined FNs with an entropy-driven DNA amplifier to construct lateral flow assay biosensor for the sensitive detection of nucleic acids. As shown in Scheme 1A, the substrate strand (S) is a three-stranded hybridization complex, which consists of a reporter strand (R) with amino modification at the 5′-end to conjugate with FNs, a linker strand (L) with biotin modification at the 5′-end to combine with SA and a by-product strand (P). The linker strand contains a single-stranded toehold as toehold 1 (Scheme 1B). When the target DNA appeared, it would bind to toehold 1 to form a four-stranded metastable complex M1, which triggers a strand-displacement reaction. Consequently, the target DNA was completely bound to the linker strand to form a three-stranded complex M2 while the by-product strand was released. Subsequently, the fuel strand was bound to toehold 2 on the linker strand and formed a four-stranded complex M3. Finally, the substrate strand was converted to a double-stranded waste complex (W) and the reporter strand was released after the strand-displacement reaction. Furthermore, the target strand was regenerated and triggered a new cycle. Scheme 1C shows the fluorescent detection of the target *via* the biosensor. The capture DNA was immobilized on the test line to hybridize with the reporter strand. The entropy-driven reaction sample, which contained the amplification product reporter strands (R) were added to the sample pad with the running buffer, and then migrated along the NC membrane by capillary action before they were captured by the capture DNA, which resulted in the accumulation of FNs on the test line. Furthermore, the excess S was captured by the SA on the control line, and thus a second band appeared. However, no reporter DNA could be obtained without the target DNA, and there was only a weak fluorescence signal on the test line.

Characterization of FNs-DNA

To study the conjugation between the reporter DNA and FNs, the DLS and zeta potential of FNs and FNs–DNA conjugates were performed, respectively. As shown in Fig. 1a, the average diameter of FNs was shifted from 136.2 nm to 145.0 nm and indicated the successful combination between reporter DNA and FNs. Furthermore, the zeta potential of FNs and FNs–DNA conjugates were investigated. As shown in Fig. 1b, the zeta potential of carboxyl-functionalized FNs became much lower after conjugation with amine-modified reporter DNA. All these

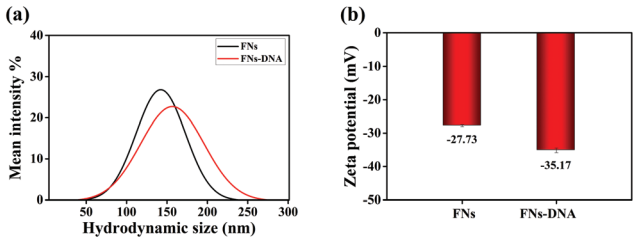

Fig. 1 Characterization of FNs-DNA. (a) The hydrodynamic diameter of FNs and FNs–DNA conjugates, (b) the zeta potential of FNs and FNs–DNA conjugates.

results indicated that the reporter DNA was successfully assembled on the surface of FNs.

The feasibility analysis of the entropy-driven DNA amplification strategy

Polyacrylamide gel electrophoresis (PAGE) experiments were performed to verify the entropy-driven DNA amplification strategy. It was shown in Fig. 2a that no obvious change in the band of the S complex (lane 6) was observed after the addition of fuel strand F, which indicated a negligible leakage. However, after the introduction of the target DNA, S was efficiently reacted with F, which caused the release of strand R (lane 5). Correspondingly, there was no obvious fluorescence signal on the test line in the absence of target DNA (Fig. 2b), while an obvious enhancement of the fluorescence signal could be seen on the test line with target DNA addition. These results indicated that this entropy-driven DNA amplification strategy was capable of detecting the target nucleic acid.

Optimization of experimental parameters

To obtain the best analytical performance of the entropy-driven DNA amplification-assisted lateral flow assay biosensor, the concentration of the capture DNA and reporter DNA, running buffer, running time, reaction temperature and entropy-driven amplified system were carefully studied. The concentration of capture DNA and reporter DNA were firstly investigated because it could directly affect the performance of the biosensor. The peak area of the test line reached the largest value when the concentration of the capture DNA and reporter DNA was 80 μM (Fig. S1†) and 2.5 μM (Fig. S2†), respectively. Therefore, 80 μM of the biotinylated capture DNA mixed with 1.0 mg mL^{-1} streptavidin and 2.5 μM of reporter DNA were selected for the following experiments. Then, we optimized the running buffer to reduce the nonspecific adsorption for ensuring a high sensitivity and good reproducibility. The result revealed that the use of PBS containing 1% Tween-20 led to the largest peak area at 30 min (Fig. S3 and S4†). In addition, the other influential factors of entropy-driven DNA amplification system were investigated, and the results showed that the maximum signal to background ratio was realized for the sensing system when the concentration ratio of stand F to S was 1.2 with an ambient reaction temperature (Fig. S5 and S6†).

The sensitivity and selectivity of the LFA biosensor

Under optimized conditions, the various concentrations of target DNA were used to evaluate the sensitivity of the biosensor. As shown in Fig. 3a, when the target DNA concentration increases from 1.5 pM to 3000 pM, a rapid increase of fluorescence intensity is observed, which agrees well with the corresponding fluorescence images of the LFA biosensors under UV light using a digital camera (Fig. 3b). Fig. 3c shows the relationship between the value of peak area and concentration of target DNA. A good linear relationship between the peak area and the concentration of target DNA ranging from 3 pM to 150 pM (R^2 = 0.9992) was obtained (Fig. 3c). The

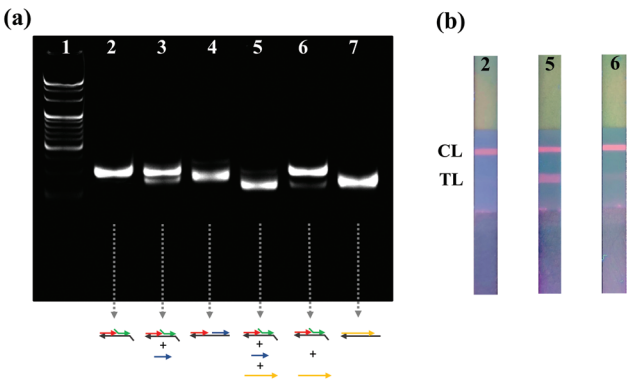

Fig. 2 (a) PAGE of entropy-driven DNA amplification strategy. Lanes 1 to 7 were marker, S, S + T, M2, S + T + F, S + F and W, (b) The photo images of LFA biosensors in the present of (1) S, (2) T + F + S, and (3) F + S.

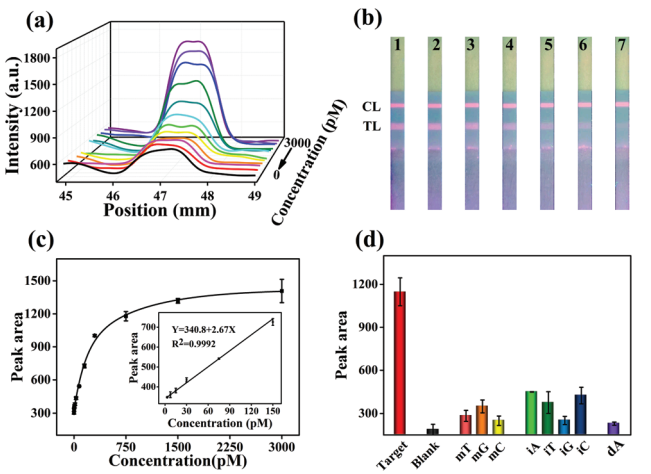

Fig. 3 The sensitivity of the LFA biosensor. (a) The fluorescent response of LFA biosensor to different concentrations of target DNA, (b) The photo images of LFA biosensor in the presence of (1) 750 pM, (2) 300 pM, (3) 150 pM, (4) 75 pM, (5) 30 pM, (6) 15 pM, (7) 0 pM target DNA, (c) the corresponding calibration curve between peak areas on the test lines and different concentrations of target DNA (inset: the responses of LFA biosensor to target DNA at low concentration), (d) selectivity toward single-base substitution (mC, mG, mT), insertion (iC, iG, iT, iA) and deletion (dA).

regression equation was peak area = 340.75 + 2.67 × [target concentration]. Based on the 3σ/slope rule, the detection limit of this biosensor was estimated to be 1.43 pM. As shown in Table S2,† the LOD of our developed entropy-driven method was 746-fold lower than that of AuNPs-labelled method (LOD = 1.0 nM). This detection sensitivity was increased 28 times and 5 times even compared to the biosensor based on RCA and HCR, respectively. These results demonstrate that the entropy-driven DNA amplifier assisted biosensor possesses high sensitivity for target detection, which holds a great potential for disease detection at an early stage.

The ability of the biosensor to discriminate target DNA from different DNA strands was then investigated, including mismatched, deleted, and inserted ones (mutant sites are shown in Table S1,† red bases). As shown in the Fig. 3d, only the target DNA produces obvious fluorescence intensity, while the other DNA sequences generate a slight signal. This result could be attributed to the difference between the breathing rates of a single base pair and two adjacent base pairs. The high selectivity suggested that the entropy-driven amplification based lateral flow assay biosensors exhibited a high potential for complex application.

The application of the designed biosensor in human serum samples

To investigate the application of the designed assay in real samples, the recovery assay was carried out in serum samples that were diluted 100 times. As shown in Table S3,† the recoveries are in the range of 95.80%–102.3% for the detection of 10 pM, 30 pM and 100 pM target DNA spiked in human serum samples with a maximum RSD of 3.7%. The above results demonstrated that the as-proposed assay held a great promise in practical applications for target DNA detection in complex samples.

To illustrate the potential of LFA biosensor as a universal sensing platform, the designed LFA was then used to detect influenza virus H1N1 RNA. Under the optimized conditions, a good response to H1N1 RNA was obtained with a detection limit of 2.02 pM (Fig. 4c), which was much lower than previously reported nanomaterial-based optical methods for H1N1 RNA detection (Table S4†). The specificity was investigated, and the result showed that the negligible change occurred in the absence of the target H1N1 RNA (Fig. 4d). Moreover, different concentrations of H1N1 RNA were added into the diluted human serum to investigate the real application of LFA biosensor. The results in Table S5† indicated that the recoveries of three serum samples at different concentrations of H1N1 RNA fluctuated slightly (95.4–101%) with the RSD values in the range of 1.4% to 4.6%. All these results suggest that the developed LFA biosensor can be used as universal platform for detecting target nucleic acids in complex samples with high sensitivity and specificity.

The stability of the LFA biosensor

Stability is another crucial parameter that should be considered in the exploitation of a new biosensor. The stability of the LFA biosensor was verified by recording the fluorescence response to target DNA after these test biosensors were stored in dry environment at 4 °C for 1 day, 1 week, 2 weeks, 1 month and 6 months. The fluorescence response and the corresponding fluorescence images of biosensors had no obvious change even after 6 months compared to that of the freshly prepared biosensor (Fig. 5a and b). The result indicated that

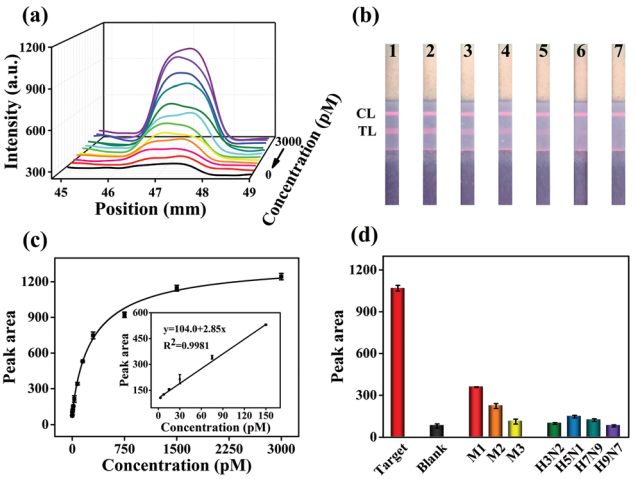

Fig. 4 The sensitivity of the biosensor for H1N1 RNA detection. (a) the fluorescent responses of biosensor to different concentrations of H1N1 RNA, (b) the photo images of LFA biosensors after addition of different concentrations of H1N1 RNA: (1) 750 pM, (2) 300 pM, (3) 150 pM, (4) 75 pM, (5) 30 pM, (6) 15 pM, (7) 0 pM, (b) the images were obtained under an UV lamp, (c) the corresponding calibration curve of peak areas on the test lines with different concentrations of H1N1 RNA (inset: the responses of the biosensor to H1N1 RNA at low concentration), (d) the selectivity of biosensor towards one-base mismatch (M1), two-base mismatch(M2), three-base mismatch(M3), H3N2, H5N1, H7N9 and H9N7.

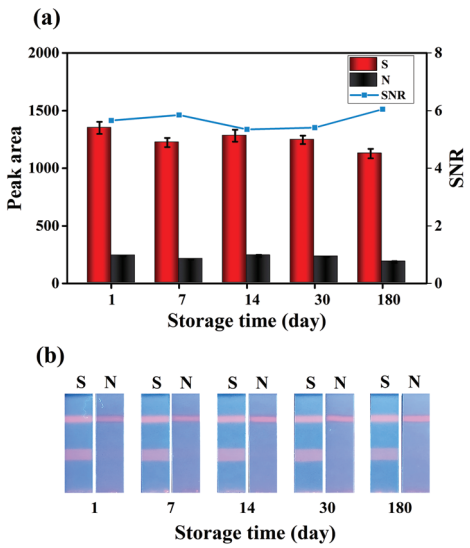

Fig. 5 Stability investigation of LFA biosensor. (a) the fluorescent responses of biosensor at different storage time, (b) the corresponding photo images of LFA biosensors.

the FNs-based LFA biosensor possessed great promise in commercial applications in the near future.

Conclusions

In summary, we have developed an entropy-driven amplification strategy assisted portable lateral flow assay biosensor for highly sensitive and selective detection of nucleic acids. The LFA biosensor possessed several distinct advantages. Using the entropy-driven amplification strategy, a superior signal-to-background ratio was obtained, which provided a high sensitivity for target nucleic acid sensing. (2) Compared with traditional nuclease-based signal amplification strategies, this enzyme-free system possessed obvious application superiority in complex biological environments. (3) The assay avoids the introduction of sophisticated equipment, complex processing procedure and the clinical laboratorian in the laboratory, making it acceptable in many resource-limited areas. We believed that the entropy-driven amplified strategy assisted biosensor may provide a new point-of-care testing platform for early disease diagnosis and treatment monitoring.

Ethics statement

The Human serum samples were provided by the First Affiliated Hospital of Zhengzhou University (Zhengzhou, China). All experiments were performed in accordance with the Guidelines of Clinical Sample Management Rules of the First Affiliated Hospital of Zhengzhou University, and approved by the Ethics Committee at the First Affiliated Hospital of Zhengzhou University. Informed consent was obtained from the blood donors of this project.

Author contributions

Shasha Li and Juan Chen: Conceptualization, data curation, formal analysis, investigation, methodology, validation, writing – original draft. Hong-Min Meng: Conceptualization, data curation, investigation, funding acquisition, resources, writing – review & editing. Hong Zong and Lin Zhang: Methodology, visualization. Zhaohui Li and Jianjun Li: Funding acquisition, resources, supervision, writing – review & editing.

Conflicts of interest

There are no conflicts to declare.

Acknowledgements

This work was supported by the National Natural Science Foundation of China (21974125 and 21605038).

References

1 J. E. van Dongen, J. T. W. Berendsen, R. D. M. Steenbergen, R. M. F. Wolthuis, J. C. T. Eijkel and L. I. Segerink, *Biosens. Bioelectron.*, 2020, **166**, 112445.
2 J. Jiao, C. Duan, L. Xue, Y. Liu, W. Sun and Y. Xiang, *Biosens. Bioelectron.*, 2020, **167**, 112479.
3 E. C. Hutchinson, *Trends Microbiol.*, 2018, **26**, 809–810.
4 V. N. Petrova and C. A. Russell, *Nat. Rev. Microbiol.*, 2018, **16**, 47–60.
5 P. L. Ho, P. H. Chau, P. S. F. Yip, G. C. Ooi, P. L. Khong, J. C. Ho, P. C. Wong, C. Ko, C. Yan and K. W. Tsang, *Eur. Respir. J.*, 2005, **26**, 474–479.
6 J. S. M. Peiris, Y. Guan and K. Y. Yuen, *Nat. Med.*, 2004, **10**, S88–S97.
7 M. P. Cheng, C. P. Yansouni, N. E. Basta, M. Desjardins, S. Kanjilal, K. Paquette, C. Caya, M. Semret, C. Quach, M. Libman, L. Mazzola, J. A. Sacks, S. Dittrich and J. Papenburg, *Ann. Intern. Med.*, 2020, **173**, 450–460.
8 F. Cui and H. S. Zhou, *Biosens. Bioelectron.*, 2020, **165**, 112349.
9 M. C. U. Cheang, M. van de Rijn and T. O. Nielsen, *Annu. Rev. Pathol.: Mech. Dis.*, 2008, **3**, 67–97.
10 H. Khalil, M. Maillet and J. D. Molkentin, *Circulation*, 2017, **136**, 1410–1411.
11 B. R. McCord, Q. Gauthier, S. Cho, M. N. Roig, G. C. Gibson-Daw, B. Young, F. Taglia, S. C. Zapico, R. F. Mariot, S. B. Lee and G. Duncan, *Anal. Chem.*, 2019, **91**, 673–688.
12 Y. Chen, N. Cheng, Y. Xu, K. Huang, Y. Luo and W. Xu, *Biosens. Bioelectron.*, 2016, **81**, 317–323.
13 Y. Chen, C. Qian, C. Liu, H. Shen, Z. Wang, J. Ping, J. Wu and H. Chen, *Biosens. Bioelectron.*, 2020, **153**, 112049.
14 R. Banerjee and A. Jaiswal, *Analyst*, 2018, **143**, 1970–1996.
15 P. Moitra, M. Alafeef, K. Dighe, M. B. Frieman and D. Pan, *ACS Nano*, 2020, **14**, 7617–7627.
16 W. Liu, M. Zhang, X. Liu, A. Sharma and X. Ding, *Biosens. Bioelectron.*, 2017, **96**, 213–219.
17 N. M. Rodriguez, J. C. Linnes, A. Fan, C. K. Ellenson, N. R. Pollock and C. M. Klapperich, *Anal. Chem.*, 2015, **87**, 7872–7879.
18 N. Kaur and B. J. Toley, *Analyst*, 2018, **143**, 2213–2234.
19 L. Liu, D. Yang and G. Liu, *Biosens. Bioelectron.*, 2019, **136**, 60–75.
20 X. Yang, J. Xie, S. Hu, W. Zhan, L. Duan, K. Chen, C. Zhang, A. Yin and M. Luo, *Sens. Actuators, B*, 2020, **311**, 127903.
21 W. Qiu, H. Xu, S. Takalkar, A. S. Gurung, B. Liu, Y. Zheng, Z. Guo, M. Baloda, K. Baryeh and G. Liu, *Biosens. Bioelectron.*, 2015, **64**, 367–372.
22 Z. Yang, C. Yi, S. Lv, Y. Sheng, W. Wen, X. Zhang and S. Wang, *Sens. Actuators, B*, 2019, **285**, 326–332.
23 W. Zheng, L. Yao, J. Teng, C. Yan, P. Qin, G. Liu and W. Chen, *Sens. Actuators, B*, 2018, **264**, 320–326.
24 M. Magiati, A. Sevastou and D. P. Kalogianni, *Microchim. Acta*, 2018, **185**, 314.

25 M. Yao, X. Lv, Y. Deng and M. Rasheed, *Anal. Chim. Acta*, 2019, **1055**, 115–125.
26 T. S. Kang, *Trends Food Sci. Technol.*, 2019, **91**, 574–585.
27 F. Couny, F. Benabid, P. J. Roberts, P. S. Light and M. G. Raymer, *Science*, 2007, **318**, 1118–1121.
28 X. Li, D. Li, W. Zhou, Y. Chai, R. Yuan and Y. Xiang, *Chem. Commun.*, 2015, **51**, 11084–11087.
29 J. Yang, B. Dou, R. Yuan and Y. Xiang, *Anal. Chem.*, 2017, **89**, 5138–5143.
30 H. M. Meng, X. Shi, J. Chen, Y. Gao, L. Qu, K. Zhang, X. B. Zhang and Z. Li, *ACS Sens.*, 2020, **5**, 103–109.
31 X. Chen, N. Briggs, J. R. McLain and A. D. Ellington, *Proc. Natl. Acad. Sci. U. S. A.*, 2013, **110**, 5386–5391.
32 P. Yin, H. M. T. Choi, C. R. Calvert and N. A. Pierce, *Nature*, 2008, **451**, 318–322.
33 R. M. Dirks and N. A. Pierce, *Proc. Natl. Acad. Sci. U. S. A.*, 2014, **101**, 15275–15278.
34 Y. Lv, L. Cui, R. Peng, Z. Zhao, L. Qiu, H. Chen, C. Jin, X. B. Zhang and W. Tan, *Anal. Chem.*, 2015, **87**, 11714–11720.
35 S. Ou, T. Xu, X. Liu, X. Yu, R. Li, J. Deng, J. Yuan and Y. Chen, *Sens. Actuators, B*, 2018, **255**, 3057–3063.
36 F. Liang, R. Lai, N. Arora, K. L. Zhang, C. C. Yeh, G. R. Barnett, P. Voigt, S. R. Corrie and R. T. Barnard, *Anal. Biochem.*, 2013, **432**, 23–30.